Heliyon 10 (2024) e26152

Contents lists available at ScienceDirect

Heliyon

journal homepage: www.cell.com/heliyon

Research article

Research on safety evaluation of collapse risk in highway tunnel construction based on intelligent fusion

Bo Wu [a,b], Yajie Wan [a,**], Shixiang Xu [a,*], Yishi Lin [c], Yonghua Huang [d], Xiaoming Lin [d], Ke Zhang [b]

[a] School of Civil and Architectural Engineering, East China University of Technology, Nanchang, 330013, Jiangxi, China
[b] College of Civil Engineering and Architecture, Guangxi University, Nanning, 530004, China
[c] Fujian Rongsheng Municipal Engineering Co., Ltd., Fuzhou, 350011, Fujian, China
[d] Lianjiang City Construction Investment Group, Fuzhou, 350011, Fujian, China

ARTICLE INFO

Keywords:
Tunnel collapse
Cloud model
D-S evidence
PSO-SVM

ABSTRACT

To solve the problems of untimely and low accuracy of tunnel project collapse risk prediction, this study proposes a method of multi-source information fusion. The method uses the PSO-SVM model to predict the surrounding rock displacement. With the prediction index as the benchmark, the Cloud Model (CM) is used to calculate the basic probability assignment value. At the same time, the improved D-S theory is used to fuse the monitoring data, the advanced geological forecast, and the tripartite information indicators of site inspection patrol. This method is applied to the risk assessment of Jinzhupa Tunnel, and the decision-makers adjust the risk factors in time according to the prediction level. In the end, the tunnel did not collapse on a large scale.

1. Introduction

At present, China is one of the countries with the largest number of highway tunnels. Road tunnels run through the different regions of communication and development. As for tunnel excavation, there are numerous risk factors involved. Complex construction processes often lead to collapse accidents. In case of collapse, it will cause casualties and social and economic losses [1,2]. Because the constitutive relationship and parameters of underground engineering soil are difficult to obtain accurately, they are often obtained by numerical simulation and field test. Wang H et al. [3] discussed the influence of parameter changes on the range of shear plastic zone of soil by limit analysis. Wang H [4] et al.determined the failure mechanism of slope soil by flume test and numerical calculation. The above methods are from the classical point of view of mechanics.

In recent years, traditional artificial intelligence methods have been widely applied in the study of risk analysis and control of tunnel collapse such as Artificial neural networks [5], Random forests [6], and Long and short-term memory neural networks [7], Gaussian regression [8], etc. However, these tools tend to be more predictive of monitoring and measuring data. The use of a single source of information to analyze the risk of the tunnel collapse, however, does not reflect the reality of the actual construction situation and leads to inaccurate assessment results. The integration of multiple sources of information is more objective in determining risk factors. While data fusion was first applied in the military field to resolve digital conflicts between different data sources [9]. Zhang

* Corresponding author.
** Corresponding author.
E-mail addresses: wanyajie1999@163.com (Y. Wan), 603559081@qq.com (S. Xu).

https://doi.org/10.1016/j.heliyon.2024.e26152
Received 6 May 2023; Received in revised form 28 November 2023; Accepted 8 February 2024
Available online 15 February 2024

et al. [10] proposed four incremental fusion mechanisms featuring changes in information sources and attributes for multi-source incomplete interval-valued data. The mechanism designs the corresponding static and dynamic fusion algorithms and the complexity of the analysis time. Thus, the computing time is reduced. Qiu et al. [11] achieved accurate identification of harvester operating conditions by a fault diagnosis algorithm based on speed fusion index, component slip rate, and adaptive threshold discrimination. Zhang et al. [12] combined the cloud model and the sequential preference similarity of ideal solutions and used the method for the Wuhan subway project example to deal with the uncertainty of coping with simulation and sensitivity analysis. Xun et al. [13] combined Building Information Modeling (BIM), Intuitionistic Fuzzy Set (IFS) theory, and D-S evidence theory for the safety risk assessment method to enhance the safety risk perception of undersea tunnel visualization. Among the above information fusion methods, the D-S evidence theory is a common approach in the field of information fusion. This is especially advantageous when distinguishing between uncertain or ambiguous decisions. However, the traditional D-S theory fusion process ignores the problem of conflicting evidence [14] and is not suitable for dealing with highly conflicting information. For example, Huang et al. [15] in the fault diagnosis of gas regulator, due to the large sample conflict coefficient, the fusion can not determine the fault state.

In addition, most of the current information fusion uses real-time monitoring data for fusion analysis, resulting in the inability to predict the occurrence of collapse accidents in advance. The excessive deformation can lead to tunnel instability and even collapse accidents. Therefore, the assessment method based on deformation prediction is an important tool to achieve intelligent warning and ensure the safety of tunnel construction.

In view of this, this paper develops a dynamic risk assessment method based on machine learning, cloud model and D-S evidence fusion. This method uses PSO-SVM algorithm to predict the displacement and deformation trend of surrounding rock, takes the predicted displacement value of surrounding rock as the information source, and integrates advanced geological prediction and on-site real-time situation. Thus, the risk level is judged, the advanced evaluation is realized, and the early warning is carried out according to the level.

2. Theory

The PSO-SVM rolling prediction is used to monitor the measurement data. Based on the predicted displacement, the cloud model + improved D-S fusion is used to calculate the basic BPA value and determine the final risk level.

2.1. CM + improved D-S evidence

The normal cloud model is a special cloud model based on Gaussian affiliation function. '*Ex*' is the central value in the field of qualitative concepts [16].

Assume that B is a qualitative concept related to X. There is a set X (1) $x \in X$ (2) x that is a random instance of concept B (3) $x \sim N(Ex, En'^2), En' \sim N(En, He^2)$, a certain degree of rank of X belonging to concept B satisfies Eq. (1):

$$\mu(x) = e^{-\frac{(x-Ex)^2}{2(En')^2}} \tag{1}$$

Analysis of tunnel envelope deformation risk factors C_i in the decision making process. To mine useful information, each risk factor should be further classified into different risk states $C_{ij}(i = 1,2,...,M; j = 1,2,...,N)$. Each risk state corresponds to a specific double limit interval, denoted as $[c_{ij}(L), c_{ij}(R)]$. The double limit interval $[c_{ij}(L), c_{ij}(R)]$ is transformed into a normal cloud model $(Ex_{ij}, En_{ij}, He_{ij})$ by Eq. (2).

The values of *Ex*, *En*, and *He* are shown below.

$$\begin{cases} Ex_{ij} \dfrac{c_{ij}(L) + c_{ij}(R)}{2} \\ En_{ij} = \dfrac{c_{ij}(R) - c_{ij}(L)}{6}, (i = 1, 2, ..., M; j = 1, 2, ..., N) \\ He_{ij} = h \end{cases} \tag{2}$$

Where "Ex_{ij}" is the expectation, "En_{ij}" is the entropy of "Ex_{ij}"; " He_{ij}" is the hyper-entropy. The distribution of "x" in the theoretical domain X is called a standard cloud. The range of the constant "h" is taken as 0.002 [17].

The basic probability distribution (BPA) of the influencing factors under different risk states can be obtained from Eq. (3).

$$\begin{cases} m_i(C_j) = \exp\left(- \dfrac{(x_i - Ex_{ij})^2}{2(En_{ij}')^2} \right) \\ \qquad\qquad , (i = 1, 2, ..., M; j = 1, 2, ..., N) \\ m_i(\Phi) = 1 - \sum_{j=1}^{N} m_i(C_j) \end{cases} \tag{3}$$

where $m_i(C_j)$ is the belief measure; En' represents a random number that satisfies $En' \sim N(En, He^2)$, and $m_i(\Phi)$ represent the BPAs value in uncertain situations; that is, the focus element cannot be determined under the indicator C_i.

The probability values obtained by fusing the indicators of the surrounding rock deformation are used to calculate the Dempster combination rule [18] for multiple evidence using Eq. (4) to obtain the risk level of each indicator.

$$\begin{cases} m(C) = \begin{cases} \dfrac{1}{1-k} \displaystyle\sum_{C_i \cap C_j \cap \cdots \cap C_k = C} m_1(C_i) m_2(C_j) \ldots m_l(C_k), \forall C \subseteq \Theta, C \neq \varnothing \\ 0, C = \varnothing \end{cases} \\ K = \displaystyle\sum_{C_i \cap C_j \cap \cdots \cap C_k = \varnothing} m_1(C_i) m_2(C_j) \ldots m_l(C_k) < 1 \end{cases} \tag{4}$$

Where the conflict factor K is defined as the normalization factor. I is the number of evidence in the combination process, and i, j, k denotes the ith, the jth, and the kth, respectively.

When the value of K converges to 1, a large conflict will arise and the evidence aggregation rule of D-S will fail. For the high conflict evidence treatment, the Jousselme distance is used to express the degree of association between the evidence source and the reference evidence, and the evidence source is corrected by Eq. (5).

$$d_{0i} = \sqrt{\frac{1}{2}(M_0 - M_i)^T D (M_0 - M_i)} \tag{5}$$

where M_0 and M_i are the reference evidence and the BPA sequence of the ith evidence, respectively, and D is a 2 N*2 N square matrix.

The correlation degree function is constructed from Eq. (6) to obtain the new evidence to calculate the fusion results.

$$\begin{cases} r_{0i} = e^{-d_{0i}}, i = 1, 2, \ldots., n (0 \leq r_{0i} \leq 1) \\ w_i = \dfrac{r_{0i}}{\sum\limits_{i=1}^{i=l} r_{0i}} \\ m_{new} = \displaystyle\sum_{i=1}^{n} w_i m_i \end{cases} \tag{6}$$

where r_{0i} and reflecting the degree of association between two pieces of evidence L are the number of evidence and the number of hypotheses, respectively.

2.2. PSO-SVM coupling algorithm process

The Support Vector Machine (SVM) is a machine learning method based on Vapnik-Chervonenk theory and structural risk minimization principle. The estimation function in the prediction process can be expressed as:

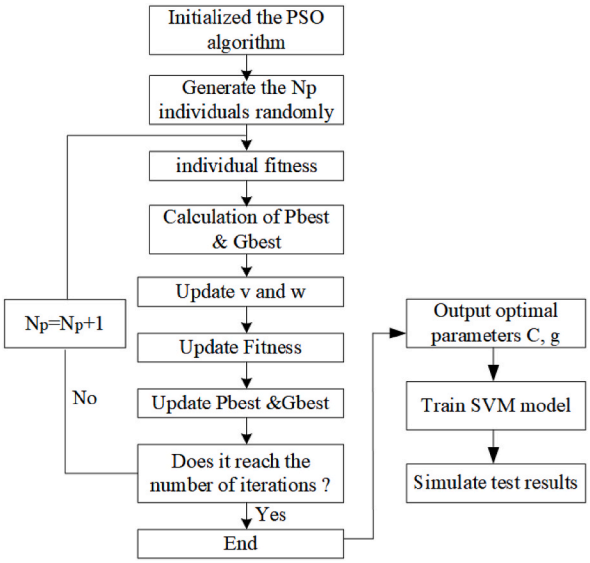

Fig. 1. PSO-SVM coupling flow chart.

$$y(x) = \sum_{n=1}^{N} w_n k(x, x_n) + w_0 \tag{7}$$

Where w_n is the weight of the model, $k(x, x_n)$ is a kernel function, w_0 and is the initial weight.

The SVM model has two critical parameters, penalty factors C and kernel function parameter g; the parameter C shows the tolerance of the model to errors, while parameter g indirectly affects the data. Compared with the traditional method, the particle swarm optimization algorithm has better global search ability and cannot easily fall into local optimum [19]. Therefore, the particle swarm optimization algorithm is used to optimize the SVM to determine the optimal hyperparameters C and g. As shown in Fig. 1, the computational procedure of the coupled PSO-SVM algorithm is as follows [20,21].

2.3. Rolling prediction algorithm

The rolling prediction method is used to predict the foundation pit displacement in this paper. Suppose the $\{x_i, y_i\}$ is used to describe the displacement [2], the number of predicted steps t, and the best historical point p. The detailed analysis is as follows.

(1) Supposing the displacement time series $\{x_i,y_i\}(i = 0,\ldots,p-1)$ have been obtained. The data of the first p days$\{x_i,y_i\}(i = 0,\ldots,p-1)$are used as the learning samples. The first prediction of rock deformation $\{x_i, y_i\}(i = p, \ldots, p+t-1)$around the pile displacement prediction on the subsequent t days is performed after completing training.
(2) For the second round, the displacement time series $\{x_i,y_i\}(i = t,\ldots,t+p-1)$ is taken as the learning sample. The t days of the data $\{x_i,y_i\}(i = t+p,\ldots,p+2t-1)$are used as the prediction samples.
(3) In the nth round of prediction, the displacement time series $\{x_i,y_i\}(i = nt,\ldots,nt+\mathrm{p}-1)$ is used as the learning sample, and the displacement $\{x_i,y_i\}(i = nt,\ldots,nt+\mathrm{p}-1)$ is predicted for the subsequent t days.

3. Multi-source heterogeneous information fusion evaluation

3.1. Case statistics and analysis

3.1.1. Project overview

The Jinzhupa Tunnel on the Puyan Expressway in Fujian Province is a two-lane split tunnel. The tunnel is designed as a two-way six-lane road with a road width of 33.5 m. The tunnel inlet uses a column type cavern door and the exit uses an end wall type cavern door. The tunnel entrance section is mainly medium-weathered siltstone, which is a softer rock. The medium-weathered rock layer is relatively broken, with a mosaic fracture structure and developed rock joints and fissures. The cave is dominated by medium-weathering siltstone, granite and powdered clay. The surrounding rocks are in bulk structure, and the self-stability of the surrounding rocks is poor; as shown in Fig. 2.

Collapse accidents are collated with reference to relevant literature [22–27], and a comprehensive analysis of 100 collapse cases is conducted. The characteristics of the composition of factors affecting tunnel collapse are shown in Fig. 3.

As shown in Fig. 3, it can be seen that there are 9 collapse factors with a ratio of 20% or more. Other factors are neglected due to their low proportion in this study. Initially, these nine risk indices are selected as the index system for tunnel collapse. Based on the literature statistics and construction experience, the risk indicators are classified and quantified as shown in Table 1.

The collected 100 datasets are used as training data. In the excavated section from ZK242 + 675 to ZK242 + 875, training samples are selected every 5 m, and 40 tunnel sections are selected as test samples. The convolutional neural network (CNN) model is used to train the collapse risk level of the test samples, and the training results are shown in Figs. 4 and 5. The numbers on the diagonal on the graph are the correct predictions, the rest are wrong predictions. The correct rate in the training sample is 94.6429%, but only 55.17% in the test sample. It may be that the visual inspection index factors do not fully reflect the overall situation of the stable surrounding rock, resulting in deviations between the assessment results alone and the actual situation. As part of the visual inspection indicators are static indicators, some of the indicators will be taken into account in the dynamic indicators of site inspections.

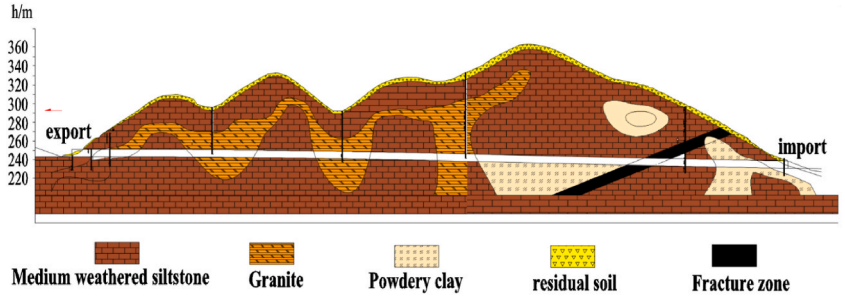

Fig. 2. Cross section of the right line of the tunnel.

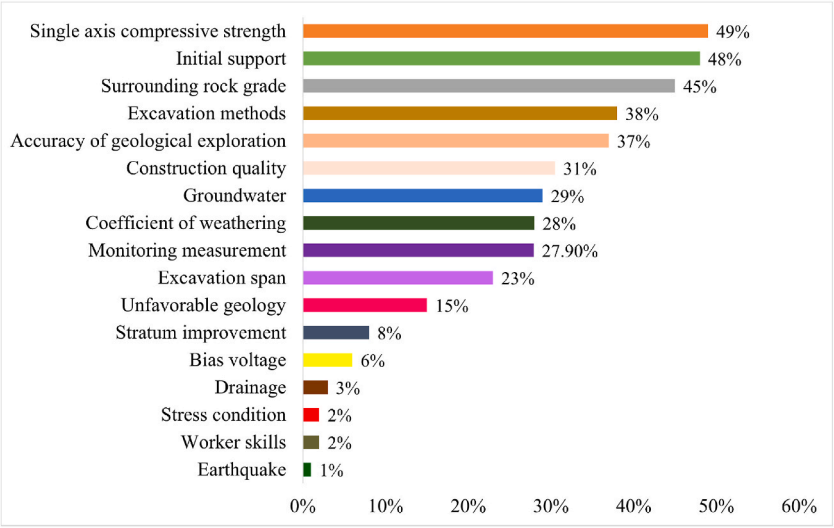

Fig. 3. Percentage of risk factors.

Table 1
Tunnel collapse deformation prediction index.

Factors	I	II	III	IV
Collapse(T)	marginal	serious	critical	catastrophic
Excavation span (m)(C1)	<7	7~10	10~14	>14
Surrounding rock grade(C2)	>550	450–550	350–450	<350
Excavation method(C3)	CRD	CD	Step method	Full-section method
Site Management(C4)	>98	95–98	92–95	88–92
Monitoring and measurement(C5)	>4	3	2	1
Initial support(C6)	Totally reasonable	Reasonable	General	Unreasonable
Weathering factor(C7)	0.9–1	0.8–0.9	0.6–0.8	0.4–0.6
Geological Survey Accuracy(C8)	>90	85–90	80–85	<80
Groundwater level(C9)	Undeveloped	General	richer	Water-rich

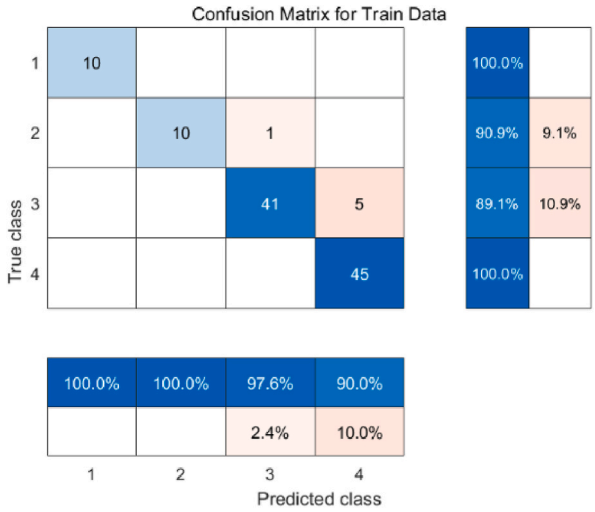

Fig. 4. Classification results of the training set.

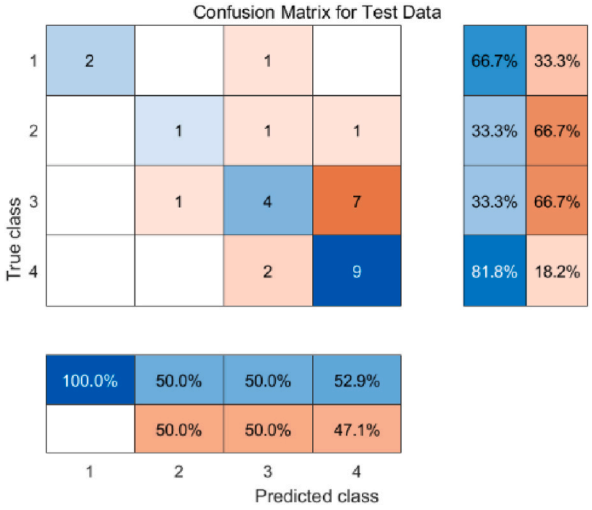

Fig. 5. Test set classification results.

3.2. Risk probability assessment

The method first collects the information from the advanced geological forecasts, on-site inspections and monitoring measurements. Then the CM is used to calculate the basic probability assignment of each information source. The overall collapse risk level is finally derived by fusing the index information through D-S evidence. The flow chart for assessing the collapse risk level is shown in Fig. 6.

3.2.1. Advanced geological forecasting

The seismic wave (TGP) is used for the advanced geological forecasting, and the original records of seismic waves are shown in Fig. 7. The offset image, estimated wave speed, SC, and R versus tunnel mileage are shown in Fig. 8. According to the TGP detection results and engineering geological analysis, the geological conditions of about 140 m (mileage 242960 m) in front of the tunnel workings can be obtained. From the right boundary of zone (2) 242870 m to the left boundary of zone (3) 242900 m, the longitudinal and transverse wave velocities remain constant [16,27].

Zhang et al. [2] established to identify potential undesirable geological units with geologically sensitive parameters in the TSP/TGP sounding results. Combined with the summary analysis of Ou, the evaluation levels based on the TGP results are shown in Table 2.

The maximum specific velocity is 0.23, and the wave axis ratio reaches 0.4. At the same time, Vp rises to 5370 m/s, and the risk probability level is II.

3.2.2. On-site inspection

The On-site inspection is an important indicator of the tunnel construction process. The inspection content is determined according to the internal and external environment stipulated in the ' Technical Specification for Monitoring of Urban Rail Transit Engineering ' GB50911-2013. Using the verification table method, the inspection content is classified and identified, and the traditional qualitative

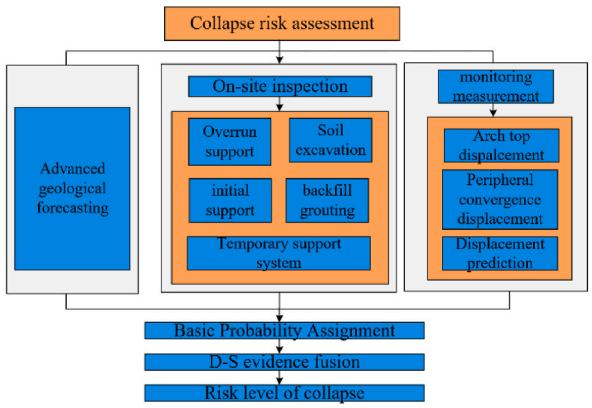

Fig. 6. The probability assessment of the risk of collapse of the tunnel construction.

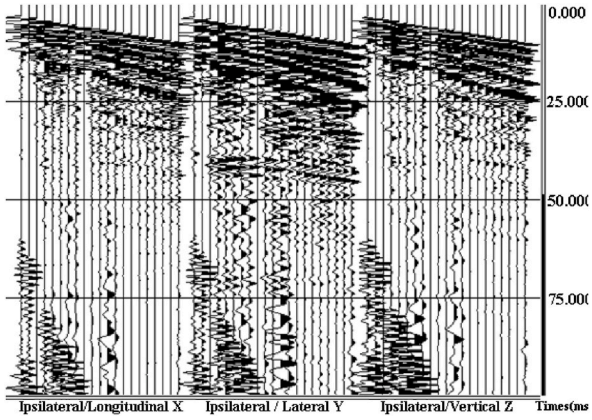

Fig. 7. Original recordings of seismic waves in three components.

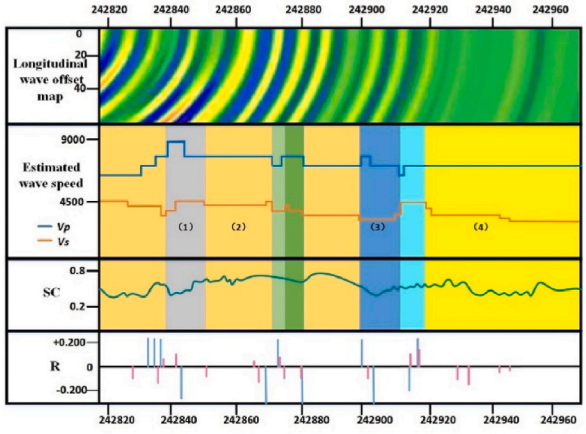

Fig. 8. Longitudinal wave offset diagram.

Table 2
Evaluation table of advance geological forecast level.

Risk probability level	I(incredible)	II(improbable)	III(remote)	IV(frequent)
TGP	(1) (2) The longitudinal and transverse wave velocities are basically constant Reflection arc ratio less than 0.06 (3) Wave axis similarity less than 0.2	(1) Small variation in longitudinal and transverse wave speed (2) Reflection arc ratio less than 0.08 (3) Wave axis similarity between 0.2 and 0.6	(1) Significant reduction in longitudinal and transverse wave speed (2) Reflection arc ratio less than 0.08 (3) Wave axis similarity greater than 0.6	(1) Significant reduction in longitudinal and transverse wave speed (2) Reflection arc ratio greater than0.08 (3) Wave axis similarity greater than 0.6

description of the risk situation in the inspection process is transformed into a semi-quantitative classification, as shown in Table 3.

3.2.3. Monitoring measurements

Monitoring measurements include vault subsidence, peripheral displacement, surface subsidence, groundwater level and blasting vibration, etc. These monitoring measurements can reflect the safety state of the surrounding rock and support structure. In this study, two indicators of vault subsidence and peripheral convergence are selected for collapse risk analysis. The daily variation amount and cumulative deformation amount are also selected as the judgment index, as shown in Table 4.

Where the cumulative deformation (y) should be based on the distance between the measurement point and the palm surface (d) multiplied by the coefficient ω.According to the Technical Specification for Monitoring and Measurement of Road Tunnels (DB 35/T 1067–2010) to determine ω, as shown in Table 5.

Table 3
Site inspection level division.

Evaluation Metrics		Risk probability level			
		I(incredible)	II(improbable)	III(remote)	IV(frequent)
Overrun support	Application of over-support	qualified	basically qualified	unqualified	complete unqualified
	Grouting effect	qualified	basically qualified	unqualified	complete unqualified
Earth excavation	Core soil size	qualified	basically qualified	unqualified	complete unqualified
	Over excavation and backfill	qualified	basically qualified	unqualified	complete unqualified
Initial support	Self-stability of the geotechnical body at the excavation face	qualified	basically qualified	unqualified	complete unqualified
	Water Leakage	dry	drip infiltration linear	Sand leakage	collapse
	Erection of longitudinal spacing	qualified	basically qualified	unqualified	complete unqualified
	Installation of locking foot anchors	qualified	basically qualified	unqualified	complete unqualified
	Stability of the initial support structure	stable	cracking	Stripping	distortion and deformation
Backfill grouting	Water leakage of the initial support structure	dry	Drip infiltration linear	femoral	karst pipeline type gushing water
Temporary support system	Temporary support structure dislocation	no displacement	slightly shifted	shifted	severe displacement
	Temporary support structure segmental removal	qualified	basically qualified	unqualified	complete unqualified

Table 4
Monitoring and measuring data classification.

Severity class of tunnel collapse	I(marginal)	II(serious)	III(critical)	IV(catastrophic)
Deformation rate(mm/d)	$0 \le x < 2$	$2 \le x < 5$	$5 \le x < 10$	$10 \le x < 20$
Cumulative deformation (mm)	$0 \le y < 50$	$50 \le y < 100$	$100 \le y < 150$	$150 \le y < 200$

Table 5
Coefficients of cumulative deformation (y) (ω).

Distance from the monitoring section to the palm face (d)	1B	2B	3B	4B~6B
ω	0.5	0.75	0.85	1

The CM eigenvalues of the monitored measurements are calculated according to Equation (3) as shown in Table 6. Meanwhile, according to the expert scoring method in Table 7 to quantify the indicators of advance geological forecasting and field inspection, the cloud model characteristic values are obtained as shown in Table 8. Each cloud droplet diagram is presented as Fig. 9(a–c).

3.2.4. Heterogeneous information fusion

(1) On-site inspections

Based on the above analysis, experts scoring are used to obtain the raw data. The initial scoring table is shown in Table 9. Based on the scoring results of the five experts, the data of each assessment index is neutralized. The basic confidence assignments (BPAs) of the assessment metrics were calculated by Eq. (1)(2) as shown in Table 10.

By improving the D-S theory and Eq. (4), the indicators are fused, and the fusion process is obtained as shown in Table 11.

(2) Monitoring measurements

The measured values of the points arranged in the cross section of tunnel ZK242 + 835 are selected, as shown in Fig. 10. Similarly, the BPA values calculated using formula (1) (2) are shown in Table 12.

The BPAs of the indicators of each measurement point in the table are fused one by one according to the evidence fusion rules of the formula mixture to obtain the final BPAs of the monitored measurement information sources. the fusion process is shown in Table 13.

It can be seen from Table 11 that when the two evidences are highly conflicting, the traditional D-S theory will fail. The improved D-S theory can correctly predict the results of the fusion model by redistributing the weights and weakening the conflict factors.

According to the "Guidelines for Construction Safety Risk Assessment of Highway Bridge and Tunnel Projects (for Trial Implementation)" (2011), the risk level criteria are divided into four levels, as shown in Fig. 11. For different levels of risk, different risk acceptance guidelines are determined for risk control, as shown in Table 14.

The tunnel collapse risk level is I according to the monitoring and measurement, while the probability level is II according to the site inspection and the probability level is II according to the advance geological forecast. The final fusion grade is moderate (Class II). It is

Table 6
CM feature values for monitoring and measuring metrics.

	Eigenvalue	I	II	III	IV
cumulative displacement	Ex	12.5	37.5	62.5	87.5
	En	8.333	8.333	8.333	8.333
	He	0.002	0.002	0.002	0.002
displacement rate	Ex	1	3.5	7.5	15
	En	0.333	0.5	0.833	1.666
	He	0.002	0.002	0.002	0.002

Table 7
Expert scoring table.

level	I	II	III	IV
score	[7.5,10]	[5,7.5]	[2.5,5]	[0,2.5]

Table 8
The CM characteristic values for advance geological forecasting and field inspection.

Eigenvalue	I	II	III	IV
Ex	8.75	6.25	3.75	1.25
En	0.416	0.416	0.416	0.416
He	0.002	0.002	0.002	0.002

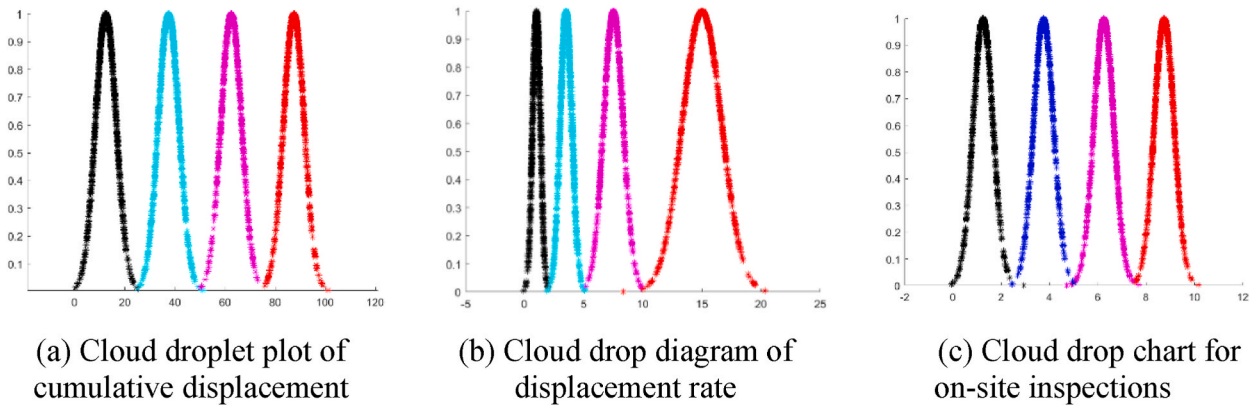

Fig. 9. Information cloud drop diagram.

Table 9
The experts' scoring table.

Evaluation Metrics		Experts'scores				
		No.1	No.2	No.3	No.4	No.5
Advance Geological Forecasting X	TGP X1	6.5	6.3	6.2	6.3	6.7
On-site inspections Y	Application of over-support Y1	6.3	6.5	6.5	5.4	6.1
	Grouting effect Y2	6.4	6.3	5.8	5.7	6.2
	Core soil size Y3	5.6	5.4	6.3	6.2	4.5
	Over excavation and backfill Y4	6.1	5.9	5.8	5.9	6.2
	Self-stability of the geotechnical body at the excavation face Y5	4.3	4.1	4.2	5.5	5.3
	Water Leakage Y6	7.2	7.1	7	7.1	7.2
	Erection of longitudinal spacing Y7	7.3	6.4	6.5	6.2	6
	Installation of locking foot anchors Y8	7.6	6.6	6.5	6.4	6.3
	Water leakage of the initial support structure Y9	5.4	5.4	5.3	5.7	5.8
	Temporary support structure dislocation Y10	6.3	6.5	6	6	6
	Temporary support structure segmental removal Y11	7.8	6.6	7.5	7.4	7

Table 10
The qualitative indicators BPA values.

	scores	I	II	III	IV
X1	6.3	0	0.9929	0.0071	0
Y1	6.3	0	0.9929	0.0071	0
Y2	6.2	0	0.9928	0.0072	0
Y3	5.6	0	0.7063	0.2936	0.001
Y4	5.9	0	0.7022	0.2978	0
Y5	4.3	0	0.002	0.4185	0.5815
Y6	7.1	0.1256	0.874	0.04	0
Y7	6.4	0	0.967	0.063	0
Y8	6.5	0	0.8354	0.1646	0
Y9	5.4	0	0.8427	0.1269	0.004
Y10	6	0	0.8337	0	0.1663
Y11	7.8	0.92	0.07	0	0

Table 11
Integration of forward geological forecasting and field inspection indicators.

The number of fusions	m(I)	m(II)	m(III)	m(IV)
1	0	0.999	0.001	0
2	0	0.9936	0.01	0
3	0	0.983	0.017	0
4	0	0.9927	0.0073	0
4	0	0.404	0.596	0
5	0	0.9368	0.063	0
6	0	0.9958	0.0042	0
7	0	0.9918	0.0082	0
8	0	0.9874	0.0126	0
9	0	1	0	0
10	0	1	0	0

The collapse risk probability level of II is obtained through the 10 fusions of on-site inspection fusion.

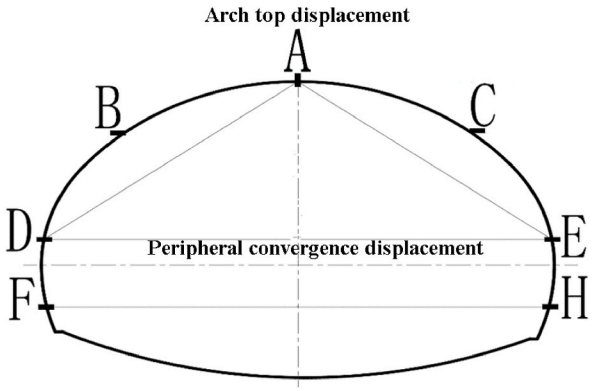

Fig. 10. Step method excavation.

in the acceptable range and does not require action, but needs to be monitored. There is no obvious crack on the surface of the exit section, and the stability of the elevation slope is good. Observation of initial support condition: The initial support of the monitored section does not show cracks and bulges, but only local dripping phenomenon. The risk level assessed is consistent with the field situation. Based on the information of monitoring and measurement, the evaluation results are different from the on-site situation. And the accuracy of the classification results of visual inspection in Fig. 5 is less than 60 %, which indicates the data uncertainty of single-source information. The multi-source information comprehensively considers all situations, so that the error result is corrected to obtain the correct prediction result.

3.3. Collapse risk control

In order to control the collapse risk ahead of time and reduce the project loss. The predicted surrounding rock displacement is used as an information source and the basic probability is redistributed. The PSO-SVM algorithm was used to roll the predicted displacement

Table 12
The BPA values for monitoring measurements.

point	index	measurements	m(I)	m(II)	m(III)	m(IV)
ZK242 + 835B	cumulative settlement value	−17.9	0.8262	0.1738	0	0
	displacement rate	−3.7	0.0771	0.9228	0	0
	D-S		0.2843	0.7157	0	0
ZK242 + 835A	cumulative settlement value	−19.1	0.7484	0.2516	0	0
	displacement rate	−4.9	0.019	0.9734	0.077	0
	D-S		0.0549	0.9451	0	0
ZK242 + 835C	cumulative settlement value	−17.6	0.8442	0.1558	0	0
	displacement rate	−4.9	0.019	0.9734	0.077	0
	D-S		0.09956	0.9044	0	0
ZK242 + 835DE	cumulative settlement value	−28.4	0.1714	0.8286	0	0
	displacement rate	−1.9	0.9681	0.026	0.0058	0
	D-S		0.8851	0.1149	0	0
ZK242 + 835FH	cumulative settlement value	−24.7	0.3577	0.6423	0	0
	Displacement rate	−1.9	0.9681	0.026	0.0058	0
	D-S		0.954	0.046	0	0

Table 13
The integration of monitoring and measurement data.

The number of fusions		m(I)	m(II)	m(III)	m(IV)
1	Improved D-S	0.0226	0.9774	0	0
	D-S	0	1	0	0
2	Improved D-S	0.025	0.9975	0	0
	D-S	0	1	0	0
3	Improved D-S	0.1618	0.8382	0	0
	D-S	0	1	0	0
4	Improved D-S	0.8001	0.1999	0	0
	D-S	–	–	–	–

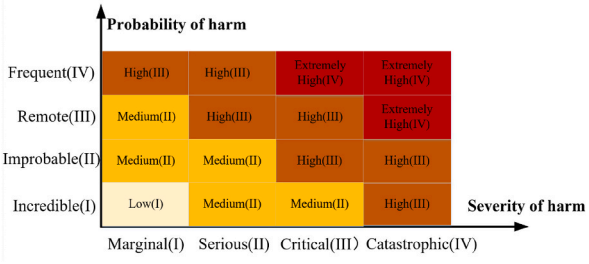

Fig. 11. Risk level criteria.

Table 14
Risk acceptance guidelines.

risk level	Acceptance guidelines	Processing measures
Low (I)	neglect	No risk measures and monitoring required
Medium (II)	accept	Generally do not need to take risk treatment measures, but need to be monitored
High (III)	Pay attention to	Risk treatment measures must be taken to reduce risk and enhance monitoring
Extremely high (IV)	High priority	High priority must be given to taking practical measures and strengthening them, or else reducing the risk to undesired levels at any cost

of the ZK242 + 835 section, and the predicted values are shown in Table 15.

Monitoring deformation collapse grade II, has been the support structure deformation. Within acceptable limits, collapses are likely to occur and require a high degree of attention. In the next three days, the deformation displacement of the surrounding rock is predicted to reach level III, with the possibility of a small collapse. Therefore, combined with the site inspection collapse risk level fusion, to determine whether the need to take risk measures. In the next three days, after the integration of site inspection indicators have been at the same level III, as shown in Table 16. The risk level of each indicator for the next three days is shown in Fig. 12.

up the progress of the tunnel. When spraying slurry for the initial support of the upper step, the cement is not strong enough due to

Table 15
Rolling forecast values.

Day	ZK835B		ZK835A		ZK835C		ZK835DE		ZK835FH	
	True	Predicted	True	Predicted	True	Predicted	True	Predicted	True	Predicted
1	−22.8	−22.6	−25.6	−24.5	−23.9	−22.8	−45.7	−43.9	−44.8	−42.4
2	−23.6	−23.1	−26.6	−24.3	−24	−23.2	−46.9	−44.7	−47.9	−42.7
3	−23.9	−23.6	−27.9	−23.9	−24.5	−23.5	−47.1	−45.2	−48.1	−41.8
4	−24.5	−24.1	−28.9	−23.4	−25.8	−23.8	−48.7	−45.6	−48.9	−40.0
5	−24.6	−23.4	−29.3	−28.8	−25.7	−24.8	−48.8	−47.6	−49.3	−46.2
6	−25.4	−22.7	−29.8	−29.5	−25.7	−25.2	−48.9	−47.8	−49.7	−43.2
7	−25.5	−22.1	−30.5	−29.7	−25.8	−25.5	−49.2	−47.7	−51.3	−41.3
8	−26.3	−21.8	−30.9	−29.5	−26	−25.7	−49.6	−47.3	−52.6	−40.5
9	−27	−25.8	−31.4	−30.5	−26.2	−25.6	−49.7	−49.4	−53.4	−52.5
10	−27.5	−26.0	−32.4	−30.4	−26.4	−25.4	−50.1	−49.3	−53.9	−53.3
11	−27.8	−26.1	−33.4	−30.0	−26.5	−25.1	−50.3	−49.0	−54.3	−53.0
12	−28.9	−26.1	−33.6	−29.4	−26.6	−24.8	−50.4	−48.6	−54.7	−51.7
MAE		6.5		7.3		3.8		3.3		9.9

$p = 11$, $t = 4$, rolling prediction after 12 days of displacement, using this displacement prediction as a benchmark to forecast the next three days of tunnel collapse. From the error point of view, both vault settlement and horizontal convergence are basically within 10%, which indicates that the algorithm has high prediction accuracy. The optimal hyperparameter results are as follows: ZK835B c = 3.9352, g = 0.1, mse = 0.014; ZK835A, c = 8.0004, g = 0.4693, mse = 0.0406; ZK835C, c = 11, g = 0.1, mse = 0.001; ZK835DE, c = 10.6461, g = 1.8925, mse = 0.0018; ZK835FH, c = 33.7722, g = 2.2973, mse = 0.0044.

Table 16
Site inspection collapse risk.

m(I)	m(II)	m(III)	m(IV)
0	0	0.9959	0.0041
0	0	0.294	0.7
0	0	0.9903	0.0097
0	0.004	0.1221	0.8775
0	0	0.9342	0.0658
0	0	0.4196	0.5804
0	0	0.9113	0.087
0	0	0.5558	0.4442
0	0	0.9291	0.0709
0	0.938	0.001	0.06
0	0	0.1456	0.8544
0	0.85057	0.19	0
0	0	1	0
0	0	0.1249	0.8747
0	0	1	0
0	0	0.5591	0.4409
0	0	1	0
0	0	0.7019	0.29
0	0	1	0

The results indicate that the collapse risk level will reach high (III) within the next 3 days. During the site inspection, it is found that the upper step excavation height is changed to 3.5 m and the upper step feed is changed to 1.9 m in order to speed.

the supply problem, and the surface is slightly cracked with dripping. Reinforcement measures for the cracked part: the cracked part of the surrounding rock is treated with slurry spraying and closed in time, as shown in Fig. 13. After the control measures are taken, the deformation rate is reduced and no large-scale collapse occurred at the site. It can be seen that the evaluation method reduces the probability of collapse risk reaching level III after the risk factors are adjusted. The timely reinforcement minimizes the probability of accidents and buys sufficient response time for decision makers. The accuracy and reliability of the method are also verified.

4. Conclusion

Relying on actual tunnel engineering, the risk assessment of heterogeneous information is carried out using data obtained from advance geological forecasts, site inspections and monitoring and measurement, and the main conclusions are obtained as follows.

(1) An improved cloud D-S evidence theory construction collapse risk probability assessment model was constructed. Improving the highly conflicting nature of D-S evidence theory in extreme cases by introducing the Jousselme distance formula. The CM is also used to determine the basic BPA values based on the advantage of the probabilistic theory based conversion between qualitative and quantitative.

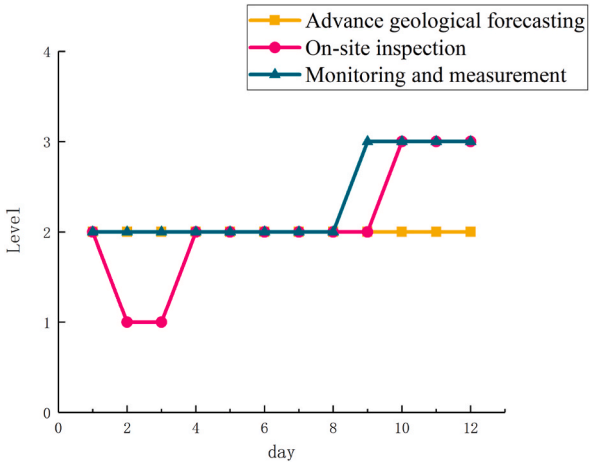

Fig. 12. Risk level of each indicator.

Fig. 13. slurry spray treatment.

(2) Based on the advance geological forecast, field inspection and monitoring and measurement data, an improved dynamic assessment model with multi-source information fusion is used. Multi-source information fusion has significant advantages in multi-attribute decision problems for construction collapse risk assessment. This method effectively improves the accuracy of assessing the probability of tunnel risk. Subsequently, the machine learning algorithms can be used to learn advanced geological prediction maps, on-site inspection pictures, etc., intelligently identify picture information and quickly classify and grade. It provides reference for the development of evaluation system and risk control system platform application.

(3) Based on the machine learning, the displacement of surrounding rock is predicted by rolling time series. It not only reduces the simulation time, but also improves the prediction efficiency and accuracy. The obtained prediction results are used as information sources to dynamically evaluate the collapse risk, and the collapse risk level is evaluated in advance to provide sufficient reaction time for decision makers, thereby improving construction efficiency.

Data availability

The data supporting the results of this study can be obtained upon request to the corresponding author.

CRediT authorship contribution statement

Bo Wu: Funding acquisition, Investigation, Methodology. **Yajie Wan:** Formal analysis, Writing – original draft. **Shixiang Xu:** Data curation, Methodology, Writing – review & editing. **Yishi Lin:** Methodology, Resources. **Yonghua Huang:** Data curation, Methodology. **Xiaoming Lin:** Methodology, Resources. **Ke Zhang:** Writing – review & editing.

Declaration of competing interest

The authors declare that they have no known competing financial interests or personal relationships that could have appeared to influence the work reported in this paper.

Acknowledgements

The authors would like to express the appreciation to the financial supports from the National Natural Science Foundation of China (No.52278397, No. 52168055), and the Natural Science Foundation of Jiangxi Province (20212ACB204001), and the 'Double Thousand Plan' Innovation Leading Talent Project of Jiangxi Province (jxsq2020101001).

References

[1] G.-H. Zhang, Y.-Y. Jiao, L.-B. Chen, H. Wang, S.-C. Li, Analytical model for assessing collapse risk during mountain tunnel construction, Can. Geotech. J. 53 (2016) 326–342, https://doi.org/10.1139/cgj-2015-0064.
[2] B. Wu, W. Qiu, W. Huang, G. Meng, Y. Nong, J. Huang, A multi-source information fusion evaluation method for the tunneling collapse disaster based on the artificial intelligence deformation prediction, Arabian J. Sci. Eng. 47 (2022) 5053–5071, https://doi.org/10.1007/s13369-021-06359-z.
[3] H. Wang, D. Fu, T. Yan, D. Pan, W. Liu, L. Ma, Bearing characteristics of multi-wing pile foundations under lateral loads in dapeng bay silty clay, JMSE 10 (2022) 1391, https://doi.org/10.3390/jmse10101391.
[4] H. Wang, Q. Hu, W. Liu, L. Ma, Z. Lv, H. Qin, J. Guo, Experimental and numerical calculation study on the slope stability of the yellow river floodplain from wantan town to liuyuankou, Toxics 11 (2023) 79, https://doi.org/10.3390/toxics11010079.
[5] J. Liu, Y. Jiang, S. Ishizu, O. Sakaguchi, Estimation of tunnel support pattern selection using artificial neural network, Arabian J. Geosci. 13 (2020) 321, https://doi.org/10.1007/s12517-020-05311-z.
[6] T. Feng, C. Wang, J. Zhang, B. Wang, Y.-F. Jin, An improved artificial bee colony-random forest (IABC-RF) model for predicting the tunnel deformation due to an adjacent foundation pit excavation, Undergr. Space 7 (2022) 514–527, https://doi.org/10.1016/j.undsp.2021.11.004.
[7] K. Liu, B. Liu, Intelligent information-based construction in tunnel engineering based on the GA and CCGPR coupled algorithm, Tunn. Undergr. Space Technol. 88 (2019) 113–128, https://doi.org/10.1016/j.tust.2019.02.012.
[8] X. Zhao, Y. Jia, A. Li, R. Jiang, Y. Song, Multi-source knowledge fusion: a survey, World Wide Web 23 (2020) 2567–2592, https://doi.org/10.1007/s11280-020-00811-0.
[9] X. Zhang, X. Chen, W. Xu, W. Ding, Dynamic information fusion in multi-source incomplete interval-valued information system with variation of information sources and attributes, Inf. Sci. 608 (2022) 1–27, https://doi.org/10.1016/j.ins.2022.06.054.
[10] Z. Qiu, G. Shi, B. Zhao, X. Jin, L. Zhou, Combine harvester remote monitoring system based on multi-source information fusion, Comput. Electron. Agric. 194 (2022) 106771, https://doi.org/10.1016/j.compag.2022.106771.
[11] L. Zhang, W. Chen, Multi-criteria group decision-making with cloud model and TOPSIS for alternative selection under uncertainty, Soft Comput. 26 (2022) 12509–12529, https://doi.org/10.1007/s00500-022-07189-3.
[12] X. Xun, J. Zhang, Y. Yuan, Multi-information fusion based on BIM and intuitionistic Fuzzy D-S evidence theory for safety risk assessment of undersea tunnel construction projects, Buildings 12 (2022) 1802, https://doi.org/10.3390/buildings12111802.
[13] Y. Zhao, J. Mi, X. Liu, X. Sun, Reconstructing images corrupted by noise based on D–S evidence theory, Int. J. Mach. Learn. & Cyber. 8 (2017) 611–618, https://doi.org/10.1007/s13042-015-0353-6.
[14] L. Ye, J. Shi, H. Ferdinando, T. Seppänen, E. Alasaarela, A multi-sensor school violence detecting method based on improved relief-F and D-S algorithms, Mobile Network. Appl. 25 (2020) 1655–1662, https://doi.org/10.1007/s11036-020-01575-7.
[15] J. Huang, Y. Wang, Fault diagnosis of gas regulator based on EWT and improved D-S evidence theory, Machine and hydraulic 51 (7) (2023) 199–207.
[16] C. Wei, J. Meng, L. Zhu, Z. Han, Assessing progress towards sustainable development goals for Chinese urban land use: a new cloud model approach, J. Environ. Manag. 326 (2023) 116826, https://doi.org/10.1016/j.jenvman.2022.116826.
[17] Y. Huang, Advances in artificial neural networks – methodological development and application, Algorithms 2 (2009) 973–1007, https://doi.org/10.3390/algor2030973.
[18] J. Cai, X. Liao, J. Bai, Z. Luo, L. Li, J. Bai, Face fatigue feature detection based on improved D-S model in complex scenes, IEEE Access 11 (2023) 101790–101798, https://doi.org/10.1109/ACCESS.2023.3314665.
[19] B.M. Sreedhara, M. Rao, S. Mandal, Application of an evolutionary technique (PSO–SVM) and ANFIS in clear-water scour depth prediction around bridge piers, Neural Comput. Appl. 31 (2019) 7335–7349, https://doi.org/10.1007/s00521-018-3570-6.
[20] L. Zhang, B. Shi, H. Zhu, X.B. Yu, H. Han, X. Fan, PSO-SVM-based deep displacement prediction of Majiagou landslide considering the deformation hysteresis effect, Landslides 18 (2021) 179–193, https://doi.org/10.1007/s10346-020-01426-2.
[21] H. Zou, J. Song, Y. Liu, etc. Prediction model of transmission line icing galloping based on PSO-SVM algorithm, [J].Vibration and shock 42 (3) (2023) 280–286.
[22] J. Sun, Research on Collapse Risk and Stability Evaluation of Surrounding Rock in Mountain Tunnel Construction by Drill and Blast method[D], Beijing Jiaotong University, 2019.
[23] L. Chen, Research on Safety Risk Evaluation Method during the Construction Period of Mountain Tunnel [D], Wuhan University, 2014.
[24] Y. Li, Research on Safety Risk Evaluation of Railroad Long Tunnel Construction [D], Chongqing Jiaotong University, 2020.
[25] F. Zhou, Research on Fuzzy Hierarchical Assessment of Collapse Risk in Mountain Tunnels[D], Zhongnan University, 2008.
[26] Y. Xue, X. Li, G. Li, et al., An analytical model for assessing soft rock tunnel collapse risk and its engineering application, Geomechanics and Engineering 23 (5) (2020) 441–454.
[27] G.-Z. Ou, Y.-Y. Jiao, G.-H. Zhang, et al., Collapse risk assessment of deep-buried tunnel during construction and its application, Tunn. Undergr. Space Technol. 115 (2021) 104019.